Conformational Substates of Myoglobin Intermediate Resolved by Picosecond X-ray Solution Scattering

Key Young Oang,[†,‡,#] Jong Goo Kim,[†,‡,#] Cheolhee Yang,[†,‡] Tae Wu Kim,[†,‡] Youngmin Kim,[†,‡] Kyung Hwan Kim,[†,‡] Jeongho Kim,[§] and Hyotcherl Ihee*[†,‡]

[†]Center for Nanomaterials and Chemical Reactions, Institute for Basic Science (IBS), Daejeon 305-701, Korea

[‡]Department of Chemistry, Graduate School of Nanoscience & Technology (WCU), Korea Advanced Institute of Science and Technology (KAIST), Daejeon 305-701, Korea

[§]Department of Chemistry, Inha University, Incheon 402-751, Korea

S *Supporting Information*

ABSTRACT: Conformational substates of proteins are generally considered to play important roles in regulating protein functions, but an understanding of how they influence the structural dynamics and functions of the proteins has been elusive. Here, we investigate the structural dynamics of sperm whale myoglobin associated with the conformational substates using picosecond X-ray solution scattering. By applying kinetic analysis considering all of the plausible candidate models, we establish a kinetic model for the entire cycle of the protein transition in a wide time range from 100 ps to 10 ms. Four structurally distinct intermediates are formed during the cycle, and most importantly, the transition from the first intermediate to the second one (**B → C**) occurs biphasically. We attribute the biphasic kinetics to the involvement of two conformational substates of the first intermediate, which are generated by the interplay between the distal histidine and the photodissociated CO.

SECTION: Biophysical Chemistry and Biomolecules
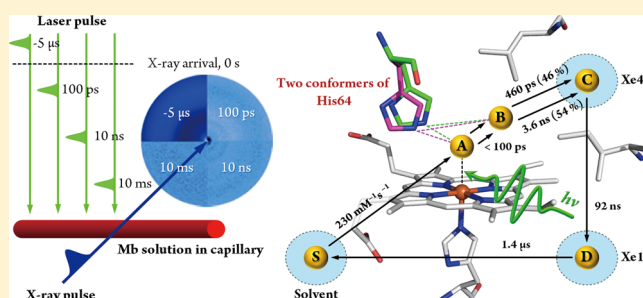
A t equilibrium, proteins in a certain state undergo continuous structural fluctuation and can exist in a number of conformational substates. In contrast, when performing their biological functions, proteins undergo non-equilibrium structural transitions from one state to another while spanning many conformational substates of each state. Such a nonequilibrium transition among the substates belonging to different states is more relevant to the protein function than the equilibrium interconversion among the substates of a given state. Because the dynamics and function of a protein are often governed by its structure, they can be presumably modulated depending on which conformational substates of a state become populated in the course of nonequilibrium protein transitions. Thus far, however, it has been challenging to determine even the dynamics of the transitions among various states let alone among conformational substates of proteins. Here, we report an example of protein structural transition where the existence of two conformational substates in a state indeed induces different kinetics in the nonequilibrium transition from the state to another.

Myoglobin (Mb) is a heme protein that transports and stores small ligands such as oxygen in muscles. Due to its small size and availability, the photosensitivity of the heme—ligand bond, and the existence of conformational substates, Mb has served as

a model system for exploring the relationships between dynamics, function, and structure of proteins.[1−7] According to infrared (IR) absorption spectra of Mb ligated with CO ligands (MbCO)[1,8] and CO-photolyzed Mb[9−12] in the frequency region of CO stretching, CO ligands move from the binding site (denoted as the **A** state) at the heme to the primary docking site (denoted as the **B** state) in the distal heme pocket in a few picoseconds.[9−12] Also, multiple stretching bands for the CO ligands in **A** and **B** states were identified, suggesting that there exist several conformational substates belonging to **A** and **B** states of the protein.[1,8−12] These bands are conventionally denoted as A_0 (1965 cm^{-1}), A_1 (1945 cm^{-1}), and A_3 (1932 cm^{-1}) for the substates of the **A** state[1,8] and B_0 (2149 cm^{-1}), B_1 (2131 cm^{-1}), and B_2 (2119 cm^{-1}) for the substates of the **B** state.[9−12] These conformational substates of **A** and **B** states arise from various conformations of distal histidine (especially its imidazole ring) in the primary docking site relative to the CO ligands.[8,10,11,13] As the CO stretching frequency is higher, the interaction between the distal histidine and the CO ligands is weaker.[11,13,14] The dynamics of equilibrium interconversion among the conformational sub-

states of MbCO were measured using ultrafast two-dimensional IR echo spectroscopy[15] and time-resolved IR spectroscopy.[14] Also, the dynamics of nonequilibrium transition among the conformational substates belonging to **A** and **B** states were estimated using time-resolved IR spectroscopy[9−11] and non-equilibrium two-dimensional IR echo spectroscopy.[12] All of these previous studies were made based on the IR absorption spectra of the protein in the frequency region of CO stretching, which are highly sensitive to the change of local structure of the protein, for example, the trajectory and the orientation of the CO ligands. However, functionally relevant, global structural change involved in these nonequilibrium transitions among conformational substates belonging to different intermediate states of Mb may be decoupled from the ligand migration and thus remain poorly understood.

In this work, we investigate the real-time structural dynamics of the transitions among intermediate states of Mb in solution. To do so, we applied picosecond X-ray solution scattering that is globally sensitive to secondary, tertiary, and quaternary structural changes of proteins in solution.[5−7,16,17] Ideally, structural refinement using the picosecond X-ray solution scattering data can reveal subtle movements of constituents such as α-helices.[5,17] However, even without such detailed structural analysis, these data can be, at the very least, treated as transient absorption (TA) spectra containing much more structural information than typical TA spectra due to intrinsic structural sensitivity of the X-ray scattering signal. From the kinetic analysis of the data, we can resolve all of the kinetic components such as the number of intermediates, their associated time constants, and the optimum kinetic model with high fidelity. Here, we focus on such kinetic aspects of the X-ray solution scattering data to assemble a puzzle of dynamics, function, and structure of proteins.

Time-resolved difference X-ray solution scattering curves, $\Delta S(q,t)$, following photoexcitation are shown in Figure 1. The measured data were analyzed by applying singular value decomposition (SVD) and kinetic analyses to extract the kinetics of the structural change of Mb. From SVD of the experimental data in the q range of 0.15−1.0 Å^{-1} and the time range of 100 ps−10 ms, four significant singular components (that is, four structurally distinct intermediates) were identified, which is consistent with previous studies using flash photolysis[18] and transient grating (TG) spectroscopy.[3] The relaxation times for these singular components were determined by simultaneously fitting four principal time-dependent singular components (right singular vectors; rSVs) multiplied by singular values using a sum of six exponentials sharing common relaxation times. From the fitting, we obtained the relaxation times of 460 ± 160 ps, 3.6 ± 0.7 ns, 92 ± 25 ns, 1.4 ± 0.2 μs, 90 ± 20 μs, and 1.2 ± 0.2 ms. Details of the SVD analysis are described in section 4.1 of the Supporting Information (SI). To verify the validity of using six exponentials for the fit, we tried to fit using fewer or more exponentials. If we use five exponentials, the fit quality clearly becomes worse, even for the most dominant first rSV component. If we use seven exponentials, overfitting occurs. Therefore, it is adequate to use six exponentials for fitting the data (see Figure S4 in the SI for details). Subsequently, the obtained relaxation times were used in the kinetic analysis based on a kinetic model.

It is clear that the last two relaxation components with the time constants of 90 μs and 1.2 ms represent the recovery of the ground-state MbCO (carbonmonoxy structure) from the last (fourth) intermediate (deoxy structure) via bimolecular
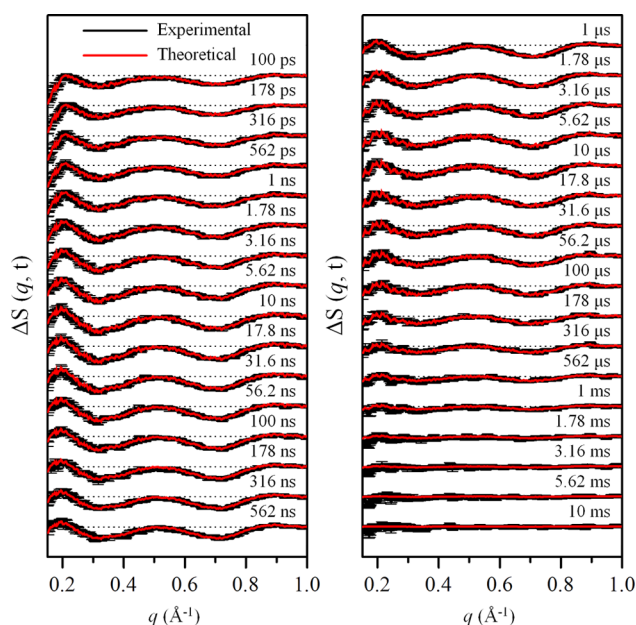
Figure 1. Time-resolved difference X-ray solution scattering curves, $\Delta S(q,t)$, measured for a solution sample of wild-type sperm whale MbCO. The time delay after photoexcitation is indicated above each curve. Experimental curves (black) are compared with theoretical curves (red) that were generated from linear combinations of four time-independent species-associated difference scattering curves extracted from the kinetic analysis using the model shown in Figure 3a.

(that is, nonexponential) nongeminate CO recombination accompanied by tertiary structural changes of the protein.[17,19,20] Then, the earlier four relaxation components must account for the multistep transitions from the first intermediate to the last one via tertiary structural changes. Because there are four relaxation components associated with the transitions among the four intermediates, one of the relaxation components must be associated with either a parallel (that is, biphasic) or bypass pathway. To identify which relaxation component is associated with such a pathway, we additionally performed the SVD analysis in a reduced time range (100 ps−3.16 ns), whose upper limit is close to the value of the second relaxation time (3.6 ns) from the above SVD analysis performed in the entire time range (100 ps−10 ms). Figures 2a and 2b show the first four left singular vectors (lSVs) in the entire time range and in the reduced time range, respectively. We can clearly see that, regardless of the time range of SVD analysis, both the first and the second lSVs in q space have significant oscillatory features. In contrast, the third and the fourth lSVs do not have any distinct features in the reduced time range. From these results of the SVD analyses, we learned that two structurally distinguishable intermediates exist in the time range from 100 ps to 3.16 ns and thus must be responsible for the first two relaxation components (460 ps and 3.6 ns).

On the basis of the results of the SVD analysis, we generated all possible kinetic models (see models **a−r** in Figure S6 in the SI). Among a total of 18 candidate models, only models **a−d** are consistent with the SVD analysis in the entire time range as well as in the reduced time range. For example, model **c** has four structurally distinct intermediates in the entire time range and two intermediates in the reduced time range, which is in agreement with the results of the SVD analyses in the two time ranges. In contrast, models **e−r** are consistent only with the SVD analysis in the entire time range. For example, model **e** has
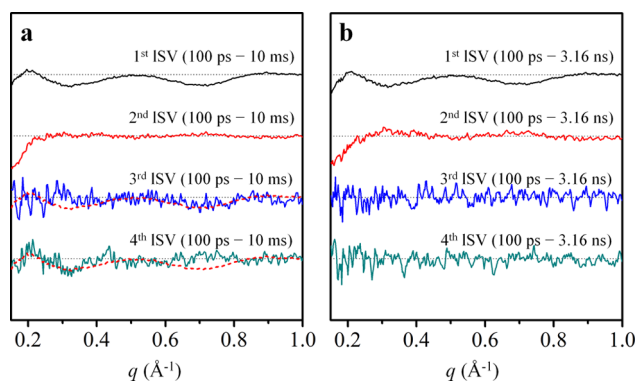
Figure 2. The result of SVD analysis in two different time ranges. (a) The first four lSVs in the entire time range (100 ps−10 ms) are shown. Four singular components of significant amplitudes were identified in the entire time range. The third and the fourth lSVs are rather noisy, but they clearly have distinct oscillatory features, as can be seen in the comparison with the first lSV (red dotted lines) superimposed on them. (b) The first four lSVs in the reduced time range (100 ps−3.16 ns) are shown. Two singular components of significant amplitudes were identified in this reduced time range.

Figure 3. The result of kinetic analysis using an optimum kinetic model. (a) The optimum kinetic model that best describes the structural dynamics of wild-type sperm whale MbCO induced by CO photolysis. (b) Population changes of the four intermediates with respect to the pump−probe time delay. The lines correspond to the populations obtained from the kinetic analysis of the experimental data, and the symbols correspond to the optimized populations at the time delay points where experimental data were measured.

four intermediates in the entire time range and three intermediates in the reduced time range, contradicting the result of the SVD analysis in the reduced time range. Then, using the four significant singular vectors obtained from the SVD analysis, we performed the kinetic analysis for each candidate kinetic model in order to determine the optimum kinetic model that best fits the experimental data. In the kinetic analysis, a theoretical time-resolved difference scattering curve (red curves in Figure 1) at each time delay was generated as a linear combination of four principal time-independent singular components in q space (that is, lSVs). The time evolution of the theoretical scattering curves can be described using a set of variable kinetic parameters based on a candidate kinetic model (for example, one of the kinetic models in Figure S6 in the SI). By minimizing the discrepancy (quantified by the χ^2 value) between the experimental and the theoretical time-resolved difference scattering curves, we optimized the kinetic parameters of each candidate kinetic model. By comparing the minimized χ^2 values (listed in Table S1 in the SI) of all of the candidate models, we determined the optimum kinetic model and extracted the species-associated difference scattering curves of the four intermediate species. Details of the kinetic analysis are described in section 4.2 of the SI.

From the kinetic analysis, we found that model **c** shown in Figure 3a gives the smallest χ^2 value among the 18 candidate models. In particular, after minimization of the χ^2 value for each candidate kinetic model, only model **c** has nonzero contribution from the parallel pathway among models **a**−**d** that have a parallel pathway in the reduced time range (100 ps− 3.16 ns), as can be seen in Figure S6 (SI). In other words, only model **c** is in agreement with the results of both SVD and kinetic analyses. Thus, we unambiguously determined that the most adequate model for describing the structural dynamics of wild-type sperm whale MbCO is model **c**. In this model, the four intermediates are termed **B**, **C**, **D**, and **S** in the order of appearance in time. Notably, this kinetic model involves (1) the biphasic transition from the first intermediate (**B**) to the second one (**C**) and (2) the bimolecular nongeminate CO recombination of the last intermediate (**S**). On the basis of the results of the kinetic analysis, the first two relaxation

components with time constants of 460 ps and 3.6 ns identified in the SVD analysis can be assigned to the biphasic transition between the **B** and **C** intermediates.

To investigate the structural dynamics of Mb in detail, we examined the time-dependent population changes of the four intermediates as shown in Figure 3b. The first intermediate (**B**) is formed within 100 ps, which is the time resolution of our experiment. In previous studies on MbCO undergoing CO photolysis under physiological conditions using time-resolved IR spectroscopy, an intermediate corresponding to **B** was observed on the time scale of several picoseconds.[10,12] In particular, two different bands of CO stretching were distinguished spectroscopically and kinetically in the transient IR spectra.[10,12] These two bands were considered to arise from the change of the histidine−CO interaction induced by two different orientations of photodissociated COs in the primary docking site, implying the existence of two conformational substates of the **B** intermediate.[9−12] It was interpreted that each substate of **B** originates from both A_1 and A_3 substates of the ground-state MbCO,[9−12] and the substates of **B** were denoted as B_1 and B_2 in the order of decreasing CO stretching frequency.[9−12] Then, we could infer that the **B** → **C** transition occurs biphasically because both B_1 and B_2 are involved in the tertiary structural relaxation associated with the **B** → **C** transition, which accompanies the movement of the photo-dissociated CO from the primary docking site to the Xe4 site.[3,21,22] According to an IR spectroscopic study by Nienhaus et al.,[11] B_1 has a higher CO stretching frequency and thus exhibits a weaker histidine−CO interaction than B_2. Therefore, the fast (460 ps) and slow (3.6 ns) relaxation components can be presumably assigned to B_1 → **C** and B_2 → **C** transitions, respectively. As can be seen in Figure 3b, the relative population ratio of these two transitions is 46/54%, with an error value of 2%. The biphasic transition from **B** to **C** has never been clearly resolved in previous studies using various spectroscopic tools,[9−12,23,24] even with time-resolved IR spectroscopy.[9−12] The lack of the biphasic transition in the time-resolved IR spectra suggests that the transition from **B** to **C** may involve both local and global structural changes of the protein because global structural changes are generally detectable only with direct structural tools.[5−7,16,17]

Following the **B** → **C** transition, **C** transforms to the third intermediate (**D**) with a time constant of 92 ns, and **D** further proceeds to the last intermediate (**S**) with a time constant of

1.4 μs. The $C \rightarrow D$ and $D \rightarrow S$ transitions correspond to tertiary structural relaxations of Mb to its deoxy structure and accompany the movements of the photodissociated CO (1) from the Xe4 site to the Xe1 site and (2) from the Xe1 site to the solvent environment, respectively.[3] For C, D, and S, no biphasic kinetics were observed. This observation implies that those intermediates do not have any conformational substates governed by the histidine−CO interaction, probably because of the escape of the photodissociated CO from the primary docking site.[3,21,22] Alternatively, if any conformational substates exist for the C, D, and S intermediates, the intrastate transitions among the substates of those intermediate states may occur much faster than the interstate transitions of $C \rightarrow D$ and $D \rightarrow S$, resulting in single-exponential dynamics of the interstate transitions.[14] Finally, S (deoxy structure) returns to the structure of the ground-state MbCO (carbonmonoxy structure) via bimolecular nongeminate CO recombination with a rate of 230 ± 10 mM^{-1} s^{-1}, which can be approximated by a combination of two unimolecular time constants of 90 μs and 1.2 ms.[17,19,20] Figure 4 summarizes the detailed scheme for the photoreaction of wild-type sperm whale MbCO, especially highlighting the movements of the CO.
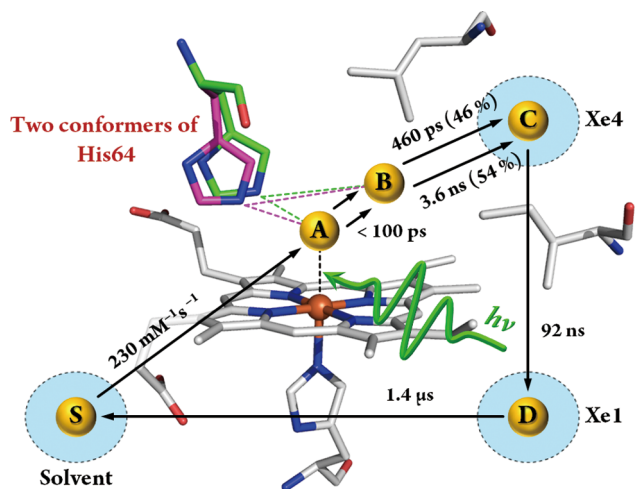
Figure 4. Detailed scheme for the photoreaction of wild-type sperm whale MbCO. In particular, the movements of the CO molecule are highlighted. Yellow spheres indicate the locations of the CO for A, B, C, D, and S states. The CO ligated to the heme (A) is dissociated by the laser pulse centered at 532 nm. The photodissociated CO moves from the primary docking site (B) via the Xe4 site (C) to the Xe1 site (D) and finally to the solvent environment (S). The interplay between the distal histidine and the CO generates the conformational substates of A and B. In particular, due to the existence of the two conformational substates of B, the transition from B to C exhibits biphasic kinetics.

The present work can be compared with previous studies on MbCO performed using time-resolved X-ray solution scattering,[5−7] as summarized in Table S2 and detailed in section 5 of the SI. A study by Kim et al.[6] investigated structural dynamics of wild-type horse heart MbCO in the time range from 100 ps to 1 μs. In contrast, our present work investigates the structural dynamics of wild-type sperm whale MbCO in a wider time range (100 ps−10 ms) than in that ref 6. A work by Cho et al.[7] is equivalent to our present work in terms of the experimental technique, sample, time range, and number of time points. The key difference between ref 7 and our present work is that ref 7

used only a sequential kinetic model while our present work considered all of the plausible candidate models (based on the SVD analysis) in the kinetic analysis to determine the optimum kinetic model with much higher fidelity. In fact, the kinetic model employed in ref 7 is identical to one of the candidate models (model r in Figure S6 in the SI) examined in our present work, and all of the evidence presented in our present work demonstrates that model r is not an optimum model.

In this work, we comprehensively elucidated the multistep structural dynamics of wild-type sperm whale MbCO induced by CO photolysis using picosecond X-ray solution scattering measured from 100 ps to 10 ms after photolysis. In particular, by combining the results of the SVD and kinetic analyses for a total of 18 candidate models, we established the most adequate kinetic model. This optimum model includes a biphasic transition from the first intermediate to the second one ($B \rightarrow C$) and bimolecular nongeminate CO recombination. Our approach of combining picosecond X-ray solution scattering, SVD analysis in variable time ranges, and subsequent kinetic analysis provides a convenient tool for determining the optimum kinetic model with high fidelity and can be further applied to other systems.

■ METHODS

Picosecond X-ray solution scattering data were acquired using the pump−probe method at the BioCARS 14-ID-B beamline at the Advanced Photon Source (APS) while the storage ring was operated in the standard top-up mode. Aqueous solution samples of wild-type sperm whale MbCO were prepared at a 8 mM concentration in 0.1 M sodium phosphate buffer at pH 7.0 using a previously established protocol. Photodissociation of MbCO was initiated by exciting the MbCO solution contained in a capillary of 1 mm thickness with a 35 ps long laser pulse at 532 nm. Subsequently, a ∼100 ps long X-ray pulse probed the sample, and the scattered X-ray photons were recorded as a function of the time delay between the laser pump pulse and the X-ray probe pulse. Time-resolved scattering curves were collected at 33 pump−probe time delays in the range from 100 ps to 10 ms (four time points per decade). Taking the difference between the scattering curve measured at each time delay point and the reference scattering curve measured at −5 μs yielded the difference scattering curve, $\Delta S(q,t)$. The contribution from laser-induced solvent heating was removed from the measured scattering curves. The details of the experiment and the data processing are provided in the SI.

■ ASSOCIATED CONTENT

Ⓢ Supporting Information

Sample preparation, data collection, data processing, data analysis, including the SVD and kinetic analyses, comparison with previous studies using time-resolved X-ray solution scattering, and related tables and figures. This material is available free of charge via the Internet at http://pubs.acs.org.

■ AUTHOR INFORMATION

Corresponding Author
*E-mail: hyotcherl.ihee@kaist.ac.kr.

Author Contributions
#K.Y.O. and J.G.K. contributed equally to this work.

Notes
The authors declare no competing financial interest.

■ REFERENCES

(1) Frauenfelder, H.; Sligar, S. G.; Wolynes, P. G. The Energy Landscapes and Motions of Proteins. *Science* **1991**, *254*, 1598−1603.

(2) Mizutani, Y.; Kitagawa, T. Ultrafast Structural Relaxation of Myoglobin Following Photodissociation of Carbon Monoxide Probed by Time-Resolved Resonance Raman Spectroscopy. *J. Phys. Chem. B* **2001**, *105*, 10992−10999.

(3) Nishihara, Y.; Sakakura, M.; Kimura, Y.; Terazima, M. The Escape Process of Carbon Monoxide from Myoglobin to Solution at Physiological Temperature. *J. Am. Chem. Soc.* **2004**, *126*, 11877−11888.

(4) Zhang, L. Y.; Wang, L. J.; Kao, Y. T.; Qiu, W. H.; Yang, Y.; Okobiah, O.; Zhong, D. P. Mapping Hydration Dynamics around a Protein Surface. *Proc. Natl. Acad. Sci. U.S.A.* **2007**, *104*, 18461−18466.

(5) Ahn, S.; Kim, K. H.; Kim, Y.; Kim, J.; Ihee, H. Protein Tertiary Structural Changes Visualized by Time-Resolved X-ray Solution Scattering. *J. Phys. Chem. B* **2009**, *113*, 13131−13133.

(6) Kim, K. H.; Oang, K. Y.; Kim, J.; Lee, J. H.; Kim, Y.; Ihee, H. Direct Observation of Myoglobin Structural Dynamics from 100 ps to 1 Microsecond with Picosecond X-ray Solution Scattering. *Chem. Commun.* **2011**, *47*, 289−291.

(7) Cho, H. S.; Dashdorj, N.; Schotte, F.; Graber, T.; Henning, R.; Anfinrud, P. Protein Structural Dynamics in Solution Unveiled via 100-ps Time-Resolved X-ray Scattering. *Proc. Natl. Acad. Sci. U.S.A.* **2010**, *107*, 7281−7286.

(8) Li, T. S.; Quillin, M. L.; Phillips, G. N.; Olson, J. S. Structural Determinants of the Stretching Frequency of CO Bound to Myoglobin. *Biochemistry* **1994**, *33*, 1433−1446.

(9) Lim, M. H.; Jackson, T. A.; Anfinrud, P. A. Mid-Infrared Vibrational Spectrum of CO after Photodissociation from Heme: Evidence for a Ligand Docking Site in the Heme Pocket of Hemoglobin and Myoglobin. *J. Chem. Phys.* **1995**, *102*, 4355−4366.

(10) Lim, M. H.; Jackson, T. A.; Anfinrud, P. A. Ultrafast Rotation and Trapping of Carbon Monoxide Dissociated from Myoglobin. *Nat. Struct. Biol.* **1997**, *4*, 209−214.

(11) Nienhaus, K.; Olson, J. S.; Franzen, S.; Nienhaus, G. U. The Origin of Stark Splitting in the Initial Photoproduct State of MbCO. *J. Am. Chem. Soc.* **2005**, *127*, 40−41.

(12) Bredenbeck, J.; Helbing, J.; Nienhaus, K.; Nienhaus, G. U.; Hamm, P. Protein Ligand Migration Mapped by Nonequilibrium 2D-IR Exchange Spectroscopy. *Proc. Natl. Acad. Sci. U.S.A.* **2007**, *104*, 14243−14248.

(13) Vojtechovsky, J.; Chu, K.; Berendzen, J.; Sweet, R. M.; Schlichting, I. Crystal Structures of Myoglobin−Ligand Complexes at Near-Atomic Resolution. *Biophys. J.* **1999**, *77*, 2153−2174.

(14) Johnson, J. B.; Lamb, D. C.; Frauenfelder, H.; Muller, J. D.; McMahon, B.; Nienhaus, G. U.; Young, R. D. Ligand Binding to Heme Proteins. VI. Interconversion of Taxonomic Substates in Carbonmonoxymyoglobin. *Biophys. J.* **1996**, *71*, 1563−1573.

(15) Ishikawa, H.; Kwak, K.; Chung, J. K.; Kim, S.; Fayer, M. D. Direct Observation of Fast Protein Conformational Switching. *Proc. Natl. Acad. Sci. U.S.A.* **2008**, *105*, 8619−8624.

(16) Konuma, T.; Kimura, T.; Matsumoto, S.; Got, Y.; Fujisawa, T.; Fersht, A. R.; Takahashi, S. Time-Resolved Small-Angle X-ray Scattering Study of the Folding Dynamics of Barnase. *J. Mol. Biol.* **2011**, *405*, 1284−1294.

(17) Kim, K. H.; Muniyappan, S.; Oang, K. Y.; Kim, J. G.; Nozawa, S.; Sato, T.; Koshihara, S. Y.; Henning, R.; Kosheleva, I.; Ki, H.; et al. Direct Observation of Cooperative Protein Structural Dynamics of Homodimeric Hemoglobin from 100 ps to 10 ms with Pump−Probe X-ray Solution Scattering. *J. Am. Chem. Soc.* **2012**, *134*, 7001−7008.

(18) Beece, D.; Eisenstein, L.; Frauenfelder, H.; Good, D.; Marden, M. C.; Reinisch, L.; Reynolds, A. H.; Sorensen, L. B.; Yue, K. T. Solvent Viscosity and Protein Dynamics. *Biochemistry* **1980**, *19*, 5147−5157.

(19) Ansari, A.; Jones, C. M.; Henry, E. R.; Hofrichter, J.; Eaton, W. A. Conformational Relaxation and Ligand Binding in Myoglobin. *Biochemistry* **1994**, *33*, 5128−5145.

(20) Balakrishnan, G.; Case, M. A.; Pevsner, A.; Zhao, X.; Tengroth, C.; McLendon, G. L.; Spiro, T. G. Time-Resolved Absorption and UV Resonance Raman Spectra Reveal Stepwise Formation of T Quaternary Contacts in the Allosteric Pathway of Hemoglobin. *J. Mol. Biol.* **2004**, *340*, 843−856.

(21) Tilton, R. F.; Kuntz, I. D.; Petsko, G. A. Cavities in Proteins: Structure of a Metmyoglobin−Xenon Complex Solved to 1.9 Å. *Biochemistry* **1984**, *23*, 2849−2857.

(22) Knapp, J. E.; Pahl, R.; Cohen, J.; Nichols, J. C.; Schulten, K.; Gibson, Q. H.; Srajer, V.; Royer, W. E., Jr. Ligand Migration and Cavities within *Scapharca* Dimeric HbI: Studies by Time-Resolved Crystallography, Xe Binding, and Computational Analysis. *Structure* **2009**, *17*, 1494−1504.

(23) Xie, X. L.; Simon, J. D. Protein Conformational Relaxation Following Photodissociation of CO from Carbonmonoxymyoglobin: Picosecond Circular Dichroism and Absorption Studies. *Biochemistry* **1991**, *30*, 3682−3692.

(24) Richard, L.; Genberg, L.; Deak, J.; Chiu, H. L.; Miller, R. J. Picosecond Phase Grating Spectroscopy of Hemoglobin and Myoglobin: Energetics and Dynamics of Global Protein Motion. *Biochemistry* **1992**, *31*, 10703−10715.

808

dx.doi.org/10.1021/jz4027425 | *J. Phys. Chem. Lett.* 2014, 5, 804−808